A Noise-Robust Method with Smoothed L1/L 2 Regularization for Sparse Moving-Source Mapping

Mai Quyen I Pham, Benoit I Oudompheng, Jerome I. Mars, Barbara Nicolas

A Noise-Robust Method with Smoothed ℓ_1/ℓ_2 Regularization for Sparse Moving-Source Mapping

Mai Quyen Pham[a,*], Benoit Oudompheng[a,b], Jérôme I. Mars[a], Barbara Nicolas[a,c]

[a] *Université Grenoble-Alpes, GIPSA-lab, F-38000 Grenoble, France*
[b] *MicrodB, 28 Chemin du Petit Bois, BP 36, 69131 Écully Cedex, France*
[c] *Université de Lyon, CREATIS, CNRS UMR5220; Inserm U1044; INSA-Lyon; Université Lyon 1, France*

Abstract

The method described here performs blind deconvolution of the beamforming output in the frequency domain. To provide accurate blind deconvolution, sparsity priors are introduced with a smoothed ℓ_1/ℓ_2 regularization term. As the mean of the noise in the power spectrum domain depends on its variance in the time domain, the proposed method includes a variance estimation step, which allows more robust blind deconvolution. Validation of the method on both simulated and real data, and of its performance, are compared with two well-known methods from the literature: the deconvolution approach for the mapping of acoustic sources, and sound density modeling.

Keywords: Smoothed ℓ_1/ℓ_2 regularization, Sparse representation, Proximal forward-backward, Acoustic moving-source localization, Beamforming blind deconvolution, Robustness algorithms.

1. Introduction

Blind deconvolution has a central role in the field of signal and image processing. It has many applications in communications [1], nondestructive testing [2], image processing [3, 4, 5], medical imaging processing [6], and in acoustics [7]. Moreover, in underwater acoustics, blind deconvolution methods have already been proposed to estimate simultaneously the transfer function of the environment and the unknown source signal in multipath underwater sound channels [8, 9, 10]. In many realistic scenarios, the blurring kernel (or the system) is imprecise or not known. Thus, the deconvolution problem becomes blind and underdetermined, and often requires additional hypotheses.

One possible additional hypothesis is the sparsity of the signal, which is an extensively studied topic in signal processing. The main idea is to find the most compact representation of a signal that consists of only a few nonzero elements. In acoustic signal processing, sparsity can be introduced either in the system or the signal domain (input). In the experimental context of this paper, the goal is to perform source mapping in a moving-source context[1]. The measurements are the pressures recorded on a horizontal line array during the pass-by experiment, and the signal of interest is the source locations inside the global vehicle. The positions of sources can be considered as sparsely distributed on a calculation grid. The question is then which measure can be used to evaluate the sparsity of a signal? In [11], Pereira used ℓ_2^2-norm as a penalty to stabilize inverse problem solutions, which can be achieved using an adapted Tikhonov regularization method. However this penalty is not adapted for the considered case of sparse source positions. An ℓ_1-norm is popular to restore the sparsity of the solution, as proposed in [12, 13]. However, in [14], Benichoux *et al.* showed that the use of the ℓ_1 norm suffers from

*Corresponding author.
Email addresses:
mai-quyen.pham@gipsa-lab.grenoble-inp.fr (Mai Quyen Pham), benoit.oudompheng@grenoble-inp.org (Benoit Oudompheng), jerome.mars@gipsa-lab.grenoble-inp.fr (Jérôme I. Mars), barbara.nicolas@creatis.insa-lyon.fr (Barbara Nicolas)

[1] In this paper the terms "source localization" and "source mapping" are equivalent. These refer to the goal of the paper, which is to map noise sources inside a global vehicle (here a boat) during a pass-by experiment.

scaling and shift ambiguities due to the nonlinear relation between the blurring kernel and the signal, as also discussed in [15, 16]. Felix *et al.* extended this result for the case of ℓ_p, $(p < 1)$-norm in [17]. In particular, both of these articles showed that using the ℓ_1/ℓ_2 function can overcome this difficulty. However, the ℓ_1/ℓ_2 function creates some difficulties when solving the nonconvex and nonsmooth minimization problems that prevent the use of such a penalty term in current restoration methods. In the present paper, we propose to use the smoothed ℓ_1/ℓ_2 ratio mentioned in [18] as a penalty. This penalty also overcomes the scaling and shift-ambiguity issues. Moreover, this ratio can be used to force the sparse representation of the signal in a blind deconvolution of moving-source mapping. Note that this is a different problem from classical blind deconvolution in underwater acoustics, as we consider several sources in a nonmultipath environment. The problem is presented in the power spectrum domain. where the noise variance is a parameter that has to be estimated jointly with the autospectra and the blur. This fundamental problem was not taken into account with the original SOOT algorithm in [18], while it is explicitly dealt with in our proposed method.

This paper is organized as follows. Following this Introduction, Section 2 is devoted to a review of the related framework for moving-source mapping using deconvolution. Section 3 presents the proposed forward model, and Section 4 describes the minimization problem, the proposed algorithm, and some mathematical tools that are essential to this methodology. The performance of the proposed method is assessed in Section 5, where we detail the chosen optimization criteria and provide comparisons with two methods: the deconvolution approach for the mapping of acoustic sources (DAMAS-MS) and the sound density modeling (SDM) methods. The proposed methodology is first evaluated on realistic synthetic data, and then it is applied to real data recorded in Lake Castillon (Verdon Gorges, France). The conclusions and perspectives are drawn up in Section 6.

2. Related work

In this section, we briefly present the classical methods that have been developed for acoustic-source localization.

Many methods have been developed to solve this problem based on array processing. The most classical one is beamforming [19], which has been extensively used due to its robustness against noise and environmental mismatch. However, classical beamforming cannot be used for pass-by experiments, where the 'vehicle' is moving and the goal is to map the different acoustic noise sources in the vehicle. Here instead, source mapping is achieved by the extension to beamforming for moving sources (BF-MS) [20].

Nevertheless, the spatial resolution of BF-MS is limited, as the image of a point source is the array transfer function, which is comprised of a main lobe and secondary lobes. Consequently, many improvements have been proposed to overcome this problem, including a hardware strategy to reduce the side-lobe levels, where the resolution of the main lobes is through optimization of the antenna geometry. In particular, several optimizations of the sensor positions of linear antennas have been proposed through the use of pseudo-random distributions [21, 22, 23]. Furthermore, a numerical strategy classically uses the weighting coefficients, which shade the array aperture and thus taper the side lobes, and as a consequence, also enlarge the main lobe [24]. Another common approach is to use deconvolution methods.

Recently, Sijtsma proposed an extended version of the deconvolution method CLEAN [25, 26] for moving sources, which is known as CLEAN-SC (*i.e.*, CLEAN based on spatial-source coherence) [27]. This method follows an approach similar to the matching pursuit method [28]. CLEAN-SC provides satisfactory results for high signal-to-noise ratios (SNRs), but requires *a-priori* knowledge of the number of sources which is not always known in practical cases. Brooks and Humphreys developed another approach, known as DAMAS [29], and its extensions [20, 30]. These algorithms use the iterative Gauss-Seidel method for solving the linear inverse problem under the nonnegative constraint on source powers. A particular extension was dedicated to moving sources, as DAMAS-MS [20], which improves moving-source mapping in the context of a high SNR. Another popular method that was also developed for moving sources is the SDM method of [31], which is based on a gradient-descent optimization technique. This represented the first use of optimization techniques with a noise prior and constraints on the signal. These two methods (*i.e.*, DAMAS-MS and SDM) will be used as the references for comparison with our proposed method.

In the case of low SNRs, the problem is difficult to solve, and thus some other approaches need to

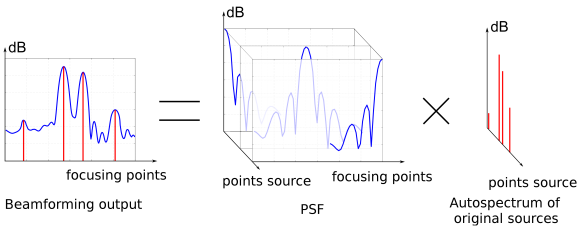

Figure 1: Modeling of the forward problem

be developed. In array processing, Swindlehurst and Kailath [32] proposed a first-order perturbation analysis of the multiple signal classification (MUSIC) and root-MUSIC algorithms for various model errors. Another possibility is to include a regularization term to stabilize the solution. The Tikhonov regularization is applied to jet noise-source localization [33]. The sparse distribution of sources is also commonly used, as in [12, 34, 35, 13, 36, 37, 38]. These methods were developed for fixed-source localization and have not currently been extended to moving sources.

The goal of the present paper is to propose a new blind deconvolution method that is applied to BF-MS results to improve moving-source mapping.

The strategy is to formulate the forward problem as an optimization problem, with constraints that are derived from the physical context. The proposed cost function contains several parts: (i) a data-fidelity term that accounts for the noise characteristics; (ii) the smoothed ℓ_1/ℓ_2 ratio [18] that promotes sparsity in the moving-source locations; and (iii) the knowledge of some physical properties of the sources and the system, and of the variance noise, introduced through indicator functions.

3. Observation model

3.1. Beamforming for moving sources

Beamforming for moving sources compensates for the Doppler effect and back-propagates the pressures measured by the M sensor array to a calculation grid of N points, which correspond to the possible source locations. We consider the classical case of pass-by experiments, in the far-field, with sources that share the same global movement and have low Mach numbers, $\|\overrightarrow{Ma}\| \ll 1$. For these conditions, some assumptions can be made over short time intervals of duration T, which are referred to as *snapshots* [20], whereby:

1) The sources are in fixed positions;

2) The Doppler effect is negligible at the frequencies and speeds of interest (*i.e.*, it does not exceed the frequency resolution defined for the localization results).

Under these assumptions, BF-MS can be implemented in a simple way in the frequency domain. The measured acoustic pressures are temporally sliced into K snapshots that are indexed by k. The calculation grid of N points is defined for the snapshot k using the *a-priori* known global trajectory of the vehicle. Note that this grid moves according to this trajectory.

For the snapshot k, the pressures measured by these M sensors at time $t \in [1, T]$ are denoted as $\check{\mathbf{p}}_t^k \in \mathbb{R}^M$, which can be divided into two parts:

$$\check{\mathbf{p}}_t^k = \check{\overline{\mathbf{p}}}_t^k + \check{\mathbf{r}}_t^k \tag{1}$$

in which $\check{\overline{\mathbf{p}}}_t^k$ are the pressures measured by the M sensors at time t for the ideal case without noise, and $\check{\mathbf{r}}_t^k$ is an additive noise in the recording domain. This defines the vectors:

$$\begin{aligned}
\check{\mathbf{P}}^k &= \left[(\check{\mathbf{p}}_1^k)^\top, (\check{\mathbf{p}}_2^k)^\top, \ldots, (\check{\mathbf{p}}_T^k)^\top\right]^\top \in \mathbb{R}^{MT}, \\
\check{\overline{\mathbf{P}}}^k &= \left[(\check{\overline{\mathbf{p}}}_1^k)^\top, (\check{\overline{\mathbf{p}}}_2^k)^\top, \ldots, (\check{\overline{\mathbf{p}}}_T^k)^\top\right]^\top \in \mathbb{R}^{MT}, \\
\check{\mathbf{R}}^k &= \left[(\check{\mathbf{r}}_1^k)^\top, (\check{\mathbf{r}}_2^k)^\top, \ldots, (\check{\mathbf{r}}_T^k)^\top\right]^\top \in \mathbb{R}^{MT},
\end{aligned}$$

where $\cdot^\top$ denotes the transpose.

We now consider the pressures measured in the frequency domain between ζ_1 and $\zeta_F\, Hz$, which is related to a vector $\mathcal{F} = [\zeta_1, \ldots, \zeta_F] \in \mathbb{R}^F$. We define the Fourier transforms of $\check{\mathbf{P}}^k$, $\check{\overline{\mathbf{P}}}^k$ and $\check{\mathbf{R}}^k$ for each snapshot k, as following:

$$\begin{aligned}
\mathbf{P}^k &= \left[(\mathbf{p}_1^k)^\top, (\mathbf{p}_2^k)^\top, \ldots, (\mathbf{p}_F^k)^\top\right]^\top \in \mathbb{C}^{MF} \\
\overline{\mathbf{P}}^k &= \left[(\overline{\mathbf{p}}_1^k)^\top, (\overline{\mathbf{p}}_2^k)^\top, \ldots, (\overline{\mathbf{p}}_F^k)^\top\right]^\top \in \mathbb{C}^{MF}, \\
\mathbf{R}^k &= \left[(\mathbf{r}_1^k)^\top, (\mathbf{r}_2^k)^\top, \ldots, (\mathbf{r}_F^k)^\top\right]^\top \in \mathbb{C}^{MF}
\end{aligned}$$

where for every $f \in \{1, \ldots, F\}$, $\mathbf{p}_f^k$, $\overline{\mathbf{p}}_f^k$, and $\mathbf{r}_f^k$ are the vectors that contain the Fourier transform coefficients $p_f^k(m), \overline{p}_f^k(m)$, and $r_f^k(m)$ of the vectors $\left[\check{\mathbf{p}}_1^k(m), \check{\mathbf{p}}_2^k(m), \ldots, \check{\mathbf{p}}_T^k(m)\right]^\top$, $\left[\check{\overline{\mathbf{p}}}_1^k(m), \check{\overline{\mathbf{p}}}_2^k(m), \ldots, \check{\overline{\mathbf{p}}}_T^k(m)\right]^\top$, and $\left[\check{\mathbf{r}}_1^k(m), \check{\mathbf{r}}_2^k(m), \ldots, \check{\mathbf{r}}_T^k(m)\right]^\top$ at the frequency $\zeta_f \in \mathcal{F}$ (ζ_f is the f^{th} element of vector $\mathcal{F}$), for

every $m \in \{1, \ldots, M\}$, respectively.

The BF-MS computed for the n^{th} calculation point at the frequency $\zeta_f \in \mathcal{F}$, and for the snapshot $k, b_f^k(n)$, is given by:

$$b_f^k(n) = |\left(\mathbf{w}_{f,n}^k\right)^{\mathsf{H}} \mathbf{p}_f^k|^2 \tag{2}$$

where $\cdot^{\mathsf{H}}$ is the conjugate transpose, and $\mathbf{w}_{f,n}^k$ is the steering vector of length M between the M sensors and the n^{th} calculation point. The m^{th} element $w_{f,n}^k(m)$ of $\mathbf{w}_{f,n}^k$ is:

$$w_{f,n}^k(m) = \left(\sum_{m'=1}^{M} \left(\frac{1}{d_{n,m'}^k}\right)^2\right)^{-1} \frac{\exp(-j\zeta_f d_{n,m}^k)}{d_{n,m}^k} \tag{3}$$

where j is the square root of -1, and $d_{n,m}^k$ is the distance between the m^{th} sensor and the n^{th} calculation point during the snapshot k. We then define the vector $\mathbf{b}_f \in \mathbb{R}^N$ with its n^{th} element $b_f(n)$ as the estimate of the BF-MS output for the n^{th} calculation point, through averaging over all of the K snapshots; *i.e.*,

$$b_f(n) = \frac{1}{K} \sum_{k=1}^{K} b_f^k(n). \tag{4}$$

Note that in the case considered, the receiver array is a linear array along the x-axis. Consequently, BF-MS is performed along the x dimension, and the calculation grid is a one-dimension vector of length N along x. For more details on these computations, we refer the reader to [39, 40].

3.2. Inverse problem formulation

We set the following assumptions:

(H1) : The sources are random variables that are mutually independent and stationary;

(H2) : The number M of the sensors is greater than the number N_s of the sources (*i.e.*, $M > N_s$), and these N_s sources are sparsely distributed on the calculation grid;

(H3) : The noise components are mutually independent, and independent of the sources.

Using the expression of the BF-MS, and assuming that the sources are located at the N points of the calculation grid, it is possible to express the BF-MS output at a given frequency ζ_f, $\mathbf{b}_f \in \mathbb{R}^N$, by:

$$\mathbf{b}_f = \mathbf{A}_f \overline{\mathbf{q}}_f + \mathbf{z}_f \tag{5}$$

where $\mathbf{A}_f \in \mathbb{R}^{N \times N}$ (Fig. 1, middle) is the array transfer function matrix that contains the beamforming point-spread functions. The $(n, n') \in \{1, \ldots, N\}^2$ element $a_f(n, n')$ of $\mathbf{A}_f$ is:

$$a_f(n, n') = \frac{1}{K} \sum_{k=1}^{K} \left| \sum_{m=1}^{M} \left(w_{f,n}^k(m)\right)^{\mathsf{H}} \frac{\exp(-j\zeta_f d_{n',m}^k)}{d_{n',m}^k} \right|^2 \tag{6}$$

$\mathbf{z}_f \in \mathbb{R}^N$ is the measurement noise, and $\overline{\mathbf{q}}_f \in \mathbb{R}^N$ is the autospectra of the possible sources located at the N calculation points (Fig. 1, right), which are the unknowns to be estimated. This expression is frequently used in deconvolution [20, 27, 31, 41], although it needs the knowledge of matrix $\mathbf{A}_f$ related to the environment and to the array to perform the deconvolution. Nowadays, some research projects are focused on uncertain cases with partially known or unknown ocean environments and experimental configurations [42]. Consequently, when $\mathbf{A}_f$ is unknown, we propose in this paper to formulate the BF-MS output at the frequency ζ_f as a blind deconvolution problem:

$$\mathbf{b}_f = \overline{\mathbf{h}}_f * \overline{\mathbf{q}}_f + \mathbf{z}_f \tag{7}$$

where $\overline{\mathbf{h}}_f \in \mathbb{R}^N$ is an unknown blur kernel, which needs to be estimated, as well as the autospectra of the sources. $*$ is a discrete-time convolution operator (with appropriate boundary processing). We now turn our attention to the term $\mathbf{z}_f$, which corresponds to the additional noise. In the literature, several methods have been proposed with $\mathbf{z}_f$ as a Gaussian noise with zero mean (which is not adapted to the BF-MS signal). We propose to introduce the noise in the time recording domain and to model its transformation throught BF-MS. In acoustics, the noise components $\check{\mathbf{r}}_{m,t}^k$ in the time domain can commonly be considered to be Gaussian, with zero mean and variance $\overline{\sigma}^2$. From Equations (1) and (2), and assumptions (H1) - (H3), we have:

$$b_f(n) = \frac{1}{K} \sum_{k=1}^{K} \left(|\left(\mathbf{w}_{f,n}^k\right)^{\mathsf{H}} \overline{\mathbf{p}}_f^k|^2 + |\left(\mathbf{w}_{f,n}^k\right)^{\mathsf{H}} \mathbf{r}_f^k|^2 \right) \tag{8}$$

Using Equation (8), we assume in this paper that the observation noise $\mathbf{z}_f$ can be divided into two terms:

$$\mathbf{z}_f = \frac{1}{K} \left(\sum_{k=1}^{K} \|\mathbf{w}_{f,n}^k\|^2 \right) \overline{\sigma}^2 \mathbb{1}_N + \mathbf{e}_f \tag{9}$$

where $\|\cdot\|$ is the ℓ_2-norm (which is also known as the Euclidean norm), $\mathbb{1}_N$ is a vector of ones of length N, and $\mathbf{e}_f \in \mathbb{R}^N$ represents the remaining unknown effects, where the amplitude of these remaining effects is much lower than that of the variance $\overline{\sigma}^2$ of the Gaussian noise. Note that:

$$\|\mathbf{w}_{f,n}^k\|^2 = \left(\sum_{m=1}^{M}\left(\frac{1}{d_{n,m}^k}\right)^2\right)^{-1}$$

Consequently, Equation (7) can be expressed as the following nonlinear problem in the standard form:

$$\mathbf{B} = \overline{\mathbf{H}} \circledast \overline{\mathbf{Q}} + \overline{\sigma}^2\delta\mathbb{1}_{NF} + \mathbf{E} \tag{10}$$

where

$$\begin{aligned}
\mathbf{B} &= \left[\mathbf{b}_1^\top, \mathbf{b}_2^\top, \ldots, \mathbf{b}_F^\top\right]^\top \in \mathbb{R}^{NF},\\
\overline{\mathbf{H}} &= \left[\overline{\mathbf{h}}_1^\top, \overline{\mathbf{h}}_2^\top, \ldots, \overline{\mathbf{h}}_F^\top\right]^\top \in \mathbb{R}^{NF},\\
\overline{\mathbf{Q}} &= \left[\overline{\mathbf{q}}_1^\top, \overline{\mathbf{q}}_2^\top, \ldots, \overline{\mathbf{q}}_F^\top\right]^\top \in \mathbb{R}^{NF},\\
\delta &= \frac{1}{K}\sum_{k=1}^{K}\left(\sum_{m=1}^{M}\left(\frac{1}{d_{n,m}^k}\right)^2\right)^{-1},\\
\mathbf{E} &= \left[\mathbf{e}_1^\top, \mathbf{e}_2^\top, \ldots, \mathbf{e}_F^\top\right]^\top \in \mathbb{R}^{NF},
\end{aligned}$$

and the discrete-time convolution operator $\circledast$ between $\overline{\mathbf{H}}$ and $\overline{\mathbf{Q}}$ is defined as follows:

$$\overline{\mathbf{H}}\circledast\overline{\mathbf{Q}} = \left[(\overline{\mathbf{h}}_1 * \overline{\mathbf{q}}_1)^\top, (\overline{\mathbf{h}}_2 * \overline{\mathbf{q}}_2)^\top, \ldots, (\overline{\mathbf{h}}_F * \overline{\mathbf{q}}_F)^\top\right]^\top.$$

4. Proposed method

4.1. Criterion to be minimized

The purpose of this study is to identify $(\overline{\mathbf{H}}, \overline{\mathbf{Q}}, \overline{\sigma}^2)$ from $\mathbf{B}$ through Equation (10), which leads to an inverse problem. To solve this, we propose the following optimization problem:

$$\text{Find } (\widehat{\mathbf{H}}, \widehat{\mathbf{Q}}, \widehat{\sigma}^2) \in \underset{\mathbf{H}\in\mathbb{R}^{2NF}, \mathbf{Q}\in\mathbb{R}^{2NF}, \sigma^2\in\mathbb{R}_+}{\operatorname{argmin}} \theta(\mathbf{H}, \mathbf{Q}, \sigma^2) \tag{11}$$

where:

$$\theta(\mathbf{H}, \mathbf{Q}, \sigma^2) = \psi(\mathbf{H}, \mathbf{Q}, \sigma^2) + \rho(\mathbf{H}, \mathbf{Q}, \sigma^2). \tag{12}$$

The first term of Equation (12) can be split into two new terms

$$\psi(\mathbf{H}, \mathbf{Q}, \sigma^2) = \phi(\mathbf{H}, \mathbf{Q}, \sigma^2) + \varphi(\mathbf{Q}), \tag{13}$$

where $\phi : \mathbb{R}^{NF} \times \mathbb{R}^{NF} \times \mathbb{R}_+ \to \mathbb{R}$ is a data fidelity term that is related to the observation model. In this case, we choose the least-squares objective function, *i.e.*,

$$\phi(\mathbf{H}, \mathbf{Q}, \sigma^2) = \frac{1}{2}\left\|\mathbf{H} \circledast \mathbf{Q} + \sigma^2\delta\mathbb{1}_{NF} - \mathbf{B}\right\|^2. \tag{14}$$

φ models a regularization function that accounts for the sparsity of the solution. In the present paper, we propose to use a new regularization function, the smoothed ℓ_1/ℓ_2 ratio, as proposed by [18]; *i.e.*, for every $\mathbf{Q} \in \mathbb{R}^{NF}$, $(\lambda, \alpha, \beta, \eta) \in]0, +\infty[^4$:

$$\varphi(\mathbf{Q}) = \lambda \log\left(\frac{\ell_{1,\alpha}(\mathbf{Q}) + \beta}{\ell_{2,\eta}(\mathbf{Q})}\right) \tag{15}$$

with,

$$\begin{aligned}
\ell_{1,\alpha}(\mathbf{Q}) &= \sum_{f=1}^{F}\sum_{n=1}^{N}\left(\sqrt{q_f(n)^2 + \alpha^2} - \alpha\right),\\
\ell_{2,\eta}(\mathbf{Q}) &= \sqrt{\sum_{f=1}^{F}\sum_{n=1}^{N} q_f(n)^2 + \eta^2}.
\end{aligned}$$

Note that empirically, the SOOT algorithm provides better results if the condition $\beta < \eta^2/\alpha$ is satisfied. The second term of Equation (12), $\rho : \mathbb{R}^{NF} \times \mathbb{R}^{NF} \times \mathbb{R}_+ \to \mathbb{R}$ is a regularization term that is related to some *a-priori* constraints on the solution. In the following, we assume that ρ can be split into three new terms that concern the three quantities to be estimated:

$$\rho(\mathbf{H}, \mathbf{Q}, \sigma^2) = \rho_1(\mathbf{H}) + \rho_2(\mathbf{Q}) + \rho_3(\sigma^2)$$

where ρ_1, ρ_2 and ρ_3 are (not necessarily smooth) proper, lower semicontinuous, convex functions [49, Ch. 1], that are continuous on their domain, and which introduce the prior knowledge on the kernel blur (system), $\mathbf{H}$, the source autospectra, $\mathbf{Q}$, and the noise variance, σ^2. Due to these properties, the problem can be addressed with the block coordinate variable metric forward-backward algorithm [44]. Moreover, in practice, $\mathbf{H}$, $\mathbf{Q}$ and σ^2 have different properties, and this choice allows the *a-priori* information to be taken into account independently from the searched quantities.

4.2. Proposed algorithm

The objective here is to provide a numerical solution to the optimization problem of Equation (12),

which is a nonlinear blind deconvolution with three unknowns $(\mathbf{H}, \mathbf{Q}, \sigma^2)$. One class of popular solutions to solve this problem is the alternating minimization algorithm, which iteratively performs the three steps: (i) updating $\mathbf{H}$ given $\mathbf{Q}$ and σ^2; (ii) updating $\mathbf{Q}$ given $\mathbf{H}$ and σ^2; and (iii) updating σ^2 given $\mathbf{H}$ and $\mathbf{Q}$ [43]. Furthermore, the criterion to minimize, which is formed as the sum of the smooth and nonsmooth functions, can be addressed with a block alternating forward-backward method [44, 45]. This method combines explicitly the (forward) gradient step with respect to the smooth (not necessarily convex) functions and the proximal (backward) step with respect to the nonsmooth functions. The convergence of the algorithm can be accelerated using a majorize-minimize approach [46, 44, 47]. In this paper, we extend the smoothed one-over-two (SOOT) algorithm proposed in [18] by including a step for the noise variance estimation. This algorithm of noise-robust SOOT (NR-SOOT) is proposed, as presented in Algorithm 1. As previously mentioned, the block-variable metric forward-backward algorithm combines two steps of the process that requires two optimization principles. We now recall the definition of these: The first is related to the choice of a variable metric that relies upon the majorization-minimization properties [47]; *i.e.*,

Definition 1 *Let $\psi : \mathbb{R}^N \to \mathbb{R}$ be a differentiable function. Let $x \in \mathbb{R}^N$. Let us define, for every $x' \in \mathbb{R}^N$:*

$$\varrho(x', x) = \psi(x) + (x - x')^\top \nabla\psi(x) + \frac{1}{2}(x - x')^\top U(x)(x - x'),$$

where $U(x) \in \mathbb{R}^{N\times N}$ is a semidefinite positive matrix. Then, $U(x)$ satisfies the majoration condition for ψ at x if $\varrho(\cdot, x)$ is a quadratic majorant of the function ψ at x; i.e., for every $x' \in \mathbb{R}^N$, $\psi(x') \leq \varrho(x', x)$.

A function ψ has a μ-Lipschitzian gradient on a convex subset $C \in \mathbb{R}^N$, with $\mu > 0$, if for every $(x, x') \in C^2$, $\|\nabla\psi(x) - \nabla\psi(x')\| \leq \mu\|x - x'\|$. Then, for every $\mathbf{x} \in C$, a quadratic majorant of ψ at $\mathbf{x}$ is easily obtained taking $U(\mathbf{x}) = \mu\, \mathrm{I}_N$, where I_N is the identity matrix of $\mathbb{R}^{N\times N}$.

The second optimization principle is the definition of the proximity operator of a proper, lower semicontinuous, convex function, relative to the metric induced by a symmetric positive definite matrix, which is defined in [48] as follows:

Definition 2 *Let $\rho : \mathbb{R}^N \to]-\infty, +\infty]$ be a proper, lower semicontinuous, and convex function, let $U \in \mathbb{R}^{N\times N}$ be a symmetric positive definite matrix, and let $x \in \mathbb{R}^N$. The proximity operator of ρ at x relative to the metric induced by U is the unique minimizer of $\rho + \frac{1}{2}(\cdot - x)^\top U(\cdot - x)$, and it is denoted by $\mathrm{prox}_{U,\rho}(x)$. If U is equal to I_N, then $\mathrm{prox}_\rho := \mathrm{prox}_{\mathrm{I}_N,\rho}$ is the proximity operator originally defined in [50].*

The convergence property of the NR-SOOT algorithm can be derived from the general results established in [44]:

Proposition 1 *Let $\left(\mathbf{Q}^l\right)_{l\in\mathbb{N}}$, $\left(\mathbf{H}^l\right)_{l\in\mathbb{N}}$ and $\left(\sigma^{2,l}\right)_{l\in\mathbb{N}}$ be sequences generated by Algorithm 1. Assume that:*

1. *There exists $(\underline{\nu}, \overline{\nu}) \in]0, +\infty[^2$ such that, for all $l \in \mathbb{N}$,*

$$\begin{aligned}
&(\forall i \in \{0, \ldots, I_l - 1\}) \\
&\qquad \underline{\nu}\,\mathrm{I}_{NF} \preceq G_1(\mathbf{H}^{l,i}, \mathbf{Q}^l, \sigma^{2,l}) \preceq \overline{\nu}\,\mathrm{I}_{NF}, \\
&(\forall j \in \{0, \ldots, J_l - 1\}) \\
&\qquad \underline{\nu}\,\mathrm{I}_{NF} \preceq G_2(\mathbf{H}^{l+1}, \mathbf{Q}^{l,j}, \sigma^{2,l}) \preceq \overline{\nu}\,\mathrm{I}_{NF}, \\
&\qquad \underline{\nu} \preceq G_3(\mathbf{H}^{l+1}, \mathbf{Q}^{l+1}, \sigma^{2,l}) \preceq \overline{\nu}.
\end{aligned}$$

2. *Step-sizes $(\gamma_1^{l,i})_{l\in\mathbb{N},0\leq i\leq I_l-1}$, $(\gamma_2^{l,j})_{l\in\mathbb{N},0\leq j\leq J_l-1}$ and $(\gamma_3^l)_{l\in\mathbb{N}}$ are chosen in the interval $[\underline{\gamma}, 2 - \overline{\gamma}]$ where $\underline{\gamma}$ and $\overline{\gamma}$ are some given positive real constants.*
3. *ρ is a semi-algebraic function.*[2]

Then, the sequence $(\mathbf{H}^l, \mathbf{Q}^l, \sigma^{2,l})_{l\in\mathbb{N}}$ converges to the critical point $(\widehat{\mathbf{H}}, \widehat{\mathbf{Q}}, \widehat{\sigma}^2)$ of Equation (11). Moreover, $\left(\theta(\mathbf{H}^l, \mathbf{Q}^l, \sigma^{2,l})\right)_{l\in\mathbb{N}}$ is a nonincreasing sequence that converges to $\theta(\widehat{\mathbf{H}}, \widehat{\mathbf{Q}}, \widehat{\sigma}^2)$.

In NR-SOOT algorithm 1, ∇_1, ∇_2, and ∇_3 are the partial gradients of ψ with respect to the variables $\mathbf{H}, \mathbf{Q}$, and σ^2. G_1, G_2, and G_3 are the semidefinite positive matrix used to build the majorizing approximations of ψ with respect to $\mathbf{H}$, $\mathbf{Q}$, and σ^2, and their expressions are given by the following proposition, as established in [18]:

[2] Semi-algebraicity is a property satisfied by a wide class of functions, which means that their graph is a finite union of sets defined by a finite number of polynomial inequalities.

Algorithm 1 The NR-SOOT algorithm.

For every $l \in \mathbb{N}$, let $I_l \in \mathbb{N}^*$, $J_l \in \mathbb{N}^*$. Let $(\gamma_1^{l,i})_{0\leq i\leq I_l-1}$, $(\gamma_2^{l,j})_{0\leq j\leq J_l-1}$, and γ_3^l be positive sequences. Initialize with $\mathbf{H}^0 \in \mathrm{dom}(\rho_1)$, $\mathbf{Q}^0 \in \mathrm{dom}(\rho_2)$, and $\sigma^{2,0} \in \mathrm{dom}(\rho_3)$.

Iterations:

For $l = 0, 1, \ldots$

$\mathbf{Q}^{l,0} = \mathbf{Q}^l,\ \mathbf{H}^{l,0} = \mathbf{H}^l,$

For $i = 0, \ldots, I_l - 1$

$\widetilde{\mathbf{H}}^{l,i+1} = \mathbf{H}^{l,i} - \gamma_1^{l,i} G_1(\mathbf{H}^{l,i}, \mathbf{Q}^l, \sigma^{2,l})^{-1} \nabla_1 \psi(\mathbf{H}^{l,i}, \mathbf{Q}^l, \sigma^{2,l})$

$\mathbf{H}^{l,i+1} = \mathrm{prox}_{(\gamma_1^{l,i})^{-1} G_1(\mathbf{H}^{l,i}, \mathbf{Q}^l, \sigma^{2,l}), \rho_1}(\widetilde{\mathbf{H}}^{l,i+1})$

$\mathbf{H}^{l+1} = \mathbf{H}^{l,I_l}$

For $j = 0, \ldots, J_l - 1$

$\widetilde{\mathbf{Q}}^{l,j+1} = \mathbf{Q}^{l,j} - \gamma_2^{l,j} G_2(\mathbf{H}^{l+1}, \mathbf{Q}^{l,j}, \sigma^{2,l})^{-1} \nabla_2 \psi(\mathbf{H}^{l+1}, \mathbf{Q}^{l,j}, \sigma^{2,l})$

$\mathbf{Q}^{l,j+1} = \mathrm{prox}_{(\gamma_2^{l,j})^{-1} G_2(\mathbf{H}^{l+1}, \mathbf{Q}^{l,j}, \sigma^{2,l}), \rho_2}(\widetilde{\mathbf{Q}}^{l,j+1})$

$\mathbf{Q}^{l+1} = \mathbf{Q}^{l,J_l}$

$\widetilde{\sigma}^{2,l} = \sigma^{2,l} - \gamma_3^l G_3(\mathbf{H}^{l+1}, \mathbf{Q}^{l+1}, \sigma^{2,l})^{-1} \nabla_3 \psi(\mathbf{H}^{l+1}, \mathbf{Q}^{l+1}, \sigma^{2,l})$

$\sigma^{2,l+1} = \mathrm{prox}_{(\gamma_3^l)^{-1} G_3(\mathbf{H}^{l+1}, \mathbf{Q}^{l+1}, \sigma^{2,l}), \rho_3}(\widetilde{\sigma}^{2,l})$

Proposition 2 *For every* $(\mathbf{H}, \mathbf{Q}, \sigma^2) \in \mathbb{R}^{NF} \times \mathbb{R}^{NF} \times \mathbb{R}_+$, *let:*

$$G_1(\mathbf{H}, \mathbf{Q}, \sigma^2) = \mu_1(\mathbf{Q}, \sigma^2)\, \mathrm{I}_{NF},$$

$$G_2(\mathbf{H}, \mathbf{Q}, \sigma^2) = \left(\mu_2(\mathbf{H}, \sigma^2) + \frac{9\lambda}{8\eta^2}\right) \mathrm{I}_{NF} + \frac{\lambda}{\ell_{1,\alpha}(\mathbf{Q}) + \beta} G_{\ell_{1,\alpha}}(\mathbf{Q}),$$

$$G_3(\mathbf{H}, \mathbf{Q}, \sigma^2) = \mu_3(\mathbf{H}, \mathbf{Q}),$$

where:

$$G_{\ell_{1,\alpha}}(\mathbf{Q}) = \mathrm{Diag}\left(\left((q_f(n)^2 + \alpha^2)^{-1/2}\right)_{1\leq f\leq F,\, 1\leq n\leq N}\right), \tag{16}$$

and $\mu_1(\mathbf{Q}, \sigma^2)$, $\mu_2(\mathbf{H}, \sigma^2)$, *and* $\mu_3(\mathbf{H}, \mathbf{Q})$ *are the Lipschitz constants for* $\nabla_1\phi(\cdot, \mathbf{Q}, \sigma^2)$, $\nabla_2\phi(\mathbf{H}, \cdot, \sigma^2)$, *and* $\nabla_3\phi(\mathbf{H}, \mathbf{Q}, \cdot)$, *respectively.*[3] *Then,* $G_1(\mathbf{H}, \mathbf{Q}, \sigma^2)$, $G_2(\mathbf{H}, \mathbf{Q}, \sigma^2))$, *and* $G_3(\mathbf{H}, \mathbf{Q}, \sigma^2)$ *satisfy the majoration condition for* $\psi(\cdot, \mathbf{Q}, \sigma^2)$ *at* $\mathbf{H}$, $\psi(\mathbf{H}, \cdot, \sigma^2)$ *at* $\mathbf{Q}$, *and* $\psi(\mathbf{H}, \mathbf{Q}, \cdot)$ *at* σ^2, *respectively.*

To conclude, we have proposed a blind deconvolution method to apply to the BF-MS that imposes sparsity on the noise acoustic-source locations. This method is validated in the next section, and compared to the classical methods of DAMAS-MS and SDM, used in acoustics for moving-source deconvolution.

[3]These Lipschitz constants are straightforward to derive since ϕ is a quadratic cost.

5. Results

We consider synthetic and real data for the method validation. The synthetic data allow the use of quantitative indicators, whereas real data only provide subjective results. For both cases, we perform comparative evaluation with the standard algorithms DAMAS-MS and SDM. In practice, the kernel blur related to the array transfer function has finite energy, and thus ρ_1 can be chosen as an indicator function of set $C = \left\{\mathbf{H} \in [h_{\min}, h_{\max}]^{NF} \mid \|\mathbf{H}\| \leq \kappa\right\}$ (equal to 0 if $\mathbf{H} \in C$, and $+\infty$ otherwise), where $\kappa > 0$, and $h_{\min}$ and $h_{\max}$ are the minimum and maximum values of $\overline{\mathbf{H}}$, respectively. In the real data case, we choose $h_{\min} = 0$ and $h_{\max} = 1$. As mentioned before, the

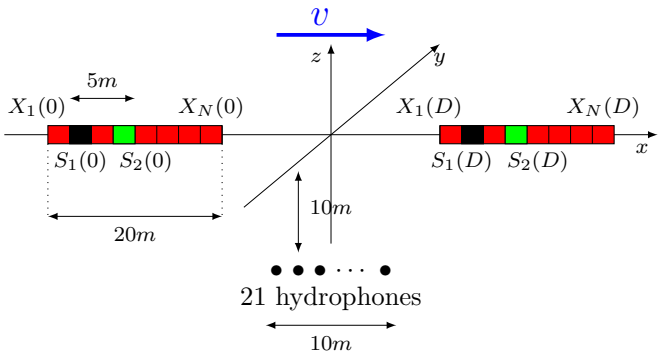

Figure 2: Simulated configuration of a pass-by experiment. Black, source S_1; green, source S_2; red, calculation grid; blue arrow, global movement of the sources.

autospectra of sources $\mathbf{Q}$ is sparse; moreover, it is limited in amplitude. Then, one natural choice for ρ_2 is the indicator function of the hypercube $[q_{\min}, q_{\max}]^{NF}$, where $q_{\min}$ (resp. $q_{\max}$) is the lower (resp., upper) boundary of $\overline{\mathbf{Q}}$. In practice, we choose $q_{\min}$ as 0, which leads to a nonnegative constraint on the source power variables, and $q_{\max}$ is the maximum value of $\mathbf{B}$. Finally, the function ρ_3 related to the constraint on the noise variance is equal to the indicator function of the interval $[\sigma^2_{\min}, \sigma^2_{\max}]$, where $\sigma^2_{\min} = 0$ and $\sigma^2_{\max} = 1$. Note that the proximity operators can be easily explicitly expressed (see Appendix).

The NR-SOOT algorithm with the penalty smoothed ℓ_1/ℓ_2 function and the classical DAMAS-MS and SDM algorithms are applied to the BF-MS result. For every $l \in \mathbb{N}$, the number of inner-loops are fixed as $I_l = 1$ and $J_l = 100$. The NR-SOOT algorithm is launched on 5000 iterations, and it can stop earlier at iteration l if $\|\mathbf{Q}^l - \mathbf{Q}^{l-1}\| \leq \sqrt{NF} \times 10^{-6}$.

5.1. Synthetic data

The simulated configuration is presented in Figure 2. Here, we consider two sources: a random broadband source located at $S_1 = (-4\,m,\, 0\,m,\, 0\,m)$ (Fig. 2, black) and a sum of 3 sine functions at frequencies $1200\,Hz$, $1400\,Hz$, and $1800\,Hz$ located at $S_2 = (1\,m,\, 0\,m,\, 0\,m)$ (Fig. 2, green), in the coordinate system where the origin is the center of the moving calculation grid all the time. The sources are moving jointly, and they follow a linear trajectory of length $20\,m$ at constant speed $v = 2\,m/s$. A linear antenna of 21 hydrophones that are equally spaced (with an inter-sensor distance of $0.5\,m$) records the propagated acoustic signals over $D = 10\,s$. Zero-mean white Gaussian noise is added to the recorded signals. To perform BF-MS, the moving calculation grid $X_n(t)$, $\forall n \in \{1, \ldots, N\}$ has a length of $20\,m$ and contains $N = 101$ points.

Concerning the initialization of the methods; $\mathbf{Q}^0$ is the BF-MS output $\mathbf{B}$. The initialization of the blur $\mathbf{H}^0$ for the SOOT and NR-SOOT algorithms is a centered Gaussian filter, such that $\mathbf{H}^0 \in C$. The regularization parameters of SDM, and $(\lambda, \alpha, \beta, \eta) \in]0, +\infty[^4$ (depending on the SOOT or NR-SOOT algorithms) are empirically adjusted, although it can be noted that the method is not too sensitive to their initialization.

Figure 3 summarizes the quantitative results in terms of reconstruction error $\overline{\mathbf{Q}}$. The relative error is defined with the ℓ_2-norm (Fig. 3, top) and

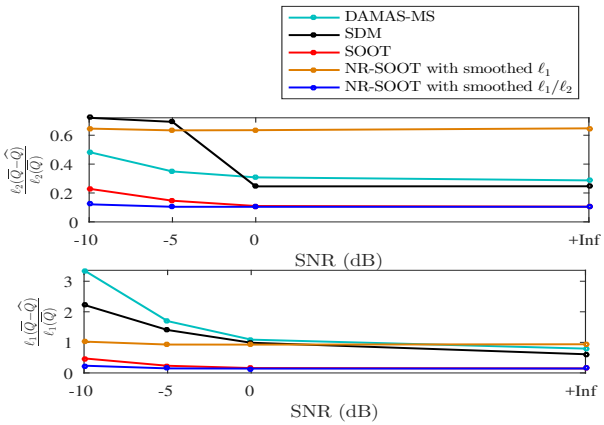

Figure 3: Comparison of the results for input data without noise and for three different signal-to-noise ratios (SNR) $\in \{-10, -5, 0\}$ dB.

ℓ_1-norm (Fig. 3, bottom) between the real $\overline{\mathbf{Q}}$ and the estimated $\widehat{\mathbf{Q}}$. It demonstrates that the method can reconstruct accurately in terms of amplitude (observing ℓ_2-norm) and in terms of sparse source positions (observing ℓ_1-norm). From Figure 3, we observe that SDM performs better in terms of source localization sparsity than DAMAS-MS for the case considered (the ℓ_1-norm values of the residual error by SDM are always smaller than those by DAMAS-MS). However, the performance of SDM decreases significantly when the SNR decreases. The NR-SOOT method with $\ell_{1,\alpha}$ as the penalty function, shown to compare $\ell_{1,\alpha}$ with ℓ_1/ℓ_2 approach, gives satisfactory results in terms of sparsity of the source localization, but not in terms of amplitude reconstruction. This result confirms the conclusion of [41], which shows that $\ell_{1,\alpha}$ should not be used in this case. The original SOOT provides very satisfying results compared to DAMAS-MS and SDM. Its performances for cases of high SNR are similar to the proposed method NR-SOOT with smoothed ℓ_1/ℓ_2. Nevertheless, for the cases of low SNR, the NR-SOOT algorithm with smoothed ℓ_1/ℓ_2 is the only one that provides a satisfactory source localization estimation. To summarize, in all of these cases, the NR-SOOT algorithm with smoothed ℓ_1/ℓ_2 as the penalty function has the smallest error for the source localization estimation in terms of sparsity and amplitude. In the following, for the NR-SOOT method, we only perform it with the smoothed ℓ_1/ℓ_2 penalty function (and call it NR-SOOT).

After this quantitative study, it is necessary to investigate the performance of these methods qualitatively, directly on the localization maps for input

data without noise and for a SNR of -10 dB. Figure 4 and Figure 5 show the results for the DAMAS-MS, SDM, original SOOT, and NR-SOOT algorithms at frequencies of 1400 Hz and 770 Hz, respectively. In these Figures, the green lines (a_1,b_1) represent the theoretical sources to estimate (in terms of position and amplitude), the magenta lines represent the BF-MS results, which are the starting points of the DAMAS-MS, SDM, original SOOT, and NR-SOOT algorithms. In Figure 4 and Figure 5, the results obtained by DAMAS-MS are in greenish-blue, those of SDM are in black (a_2,b_2), those of original SOOT are in red, and those of NR-SOOT are in blue (a_3,b_3).

At the frequency of 1400 Hz (Fig. 4), for which both sources exist, for the case without noise on the recorded data (Fig. 4a) both the original SOOT and the NR-SOOT algorithms detect the source positions accurately. DAMAS-MS gives some false alarms at $x = -3\,m$ and $x = 2.5\,m$. These false sources have small amplitudes, but they are a real problem because the number of sources is generally unknown. SDM locates two sources, but the amplitude estimation is not satisfactory and these sources are spread in the space. For the case of a SNR of -10 dB, DAMAS-MS does not succeed at all, and it shows several false alarms with significant amplitudes. With the SDM method, there is one false alarm around $x = -1\,m$, and the amplitudes are not correct. The original SOOT algorithm gives good results, although there are two false alarms around $x = -9\,m$ and $x = 9\,m$. In contrast, the NR-SOOT algorithm gives perfect results in terms of localization and source amplitude estimation.

We now turn our attention to the case at the low frequency 770 Hz (Fig. 5), for which only the source S_1 exists. In this case, DAMAS-MS and SDM give unsatisfactory results, with a spatially extended source and false alarms even in the noise-free case for DAMAS-MS. The original SOOT gives satisfactory results without noise (Fig. $5a_3$), although when the SNR decreases, the original SOOT algorithm creates false alarms (Fig. $5b_3$), while the NR-SOOT algorithm shows excellent results in terms of position and amplitude (Fig. $5b_3$). The NR-SOOT algorithm is robust against noise. In the following, for the sake of simplicity, and as it always provides the best results, we only consider the NR-SOOT algorithm for blind deconvolution of the two-dimensional illustrations.

The two-dimensional localization maps are shown in Figure 7 (without noise) and Figure 8 (SNR of -10 dB), with each Figure showing the initial BF-MS

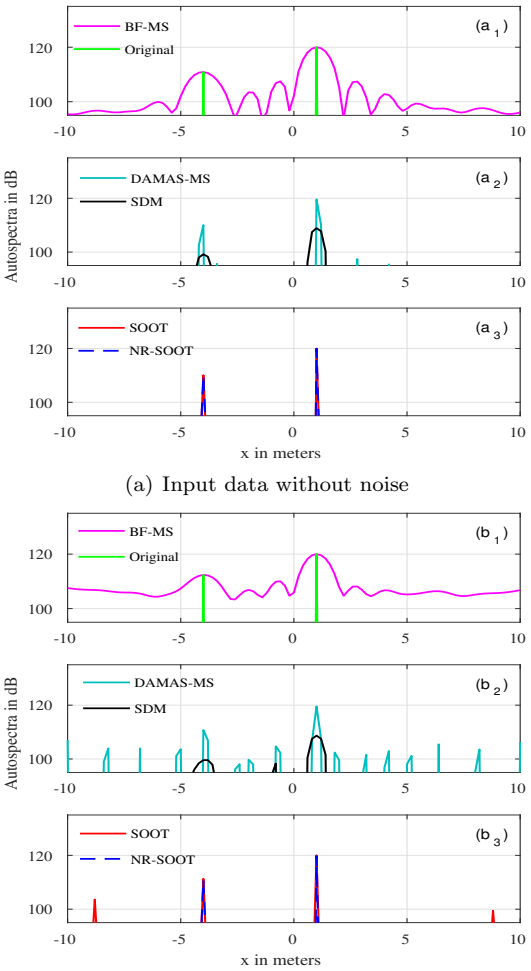

(a) Input data without noise

(b) Input data with SNR of -10 dB

Figure 4: Comparison of the results at the frequency of 1400 Hz, without noise (a), and with SNR of -10 dB (b).

and the results obtained by DAMAS-MS, SDM, original SOOT, and NR-SOOT. For the case without noise of Figure 7, all of the methods improve the BF-MS output, localize the two sources, and allow identification as one broadband source and a sum-of-sine source. However, the results obtained using DAMAS-MS and SDM are not as good as those using the original SOOT or NR-SOOT algorithms, because the source localizations are spread over several x positions. Moreover, by studying the different zones indicated in the red ellipses in Figure 7 and Figure 8, which are related to the autospectrum of the sine source at the three frequencies of 1200 Hz, 1400 Hz, and 1800 Hz, some other conclusions can be drawn. The results obtained using the DAMAS-MS method are not performing well, as some noise

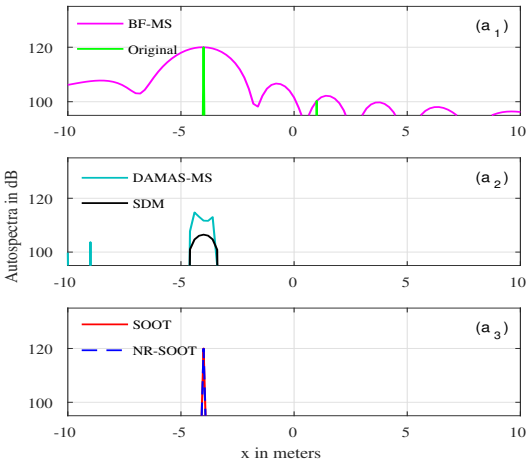

(a) Input data without noise

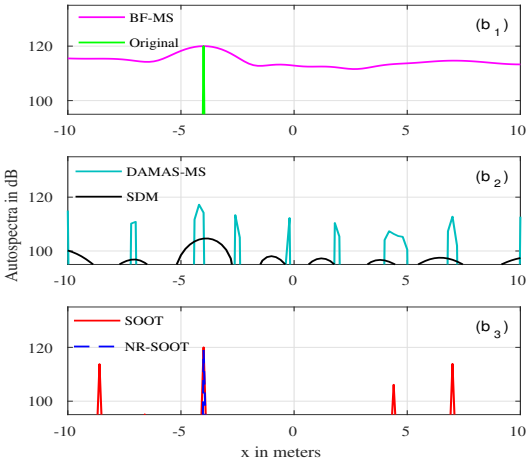

(b) Input data with SNR of -10 dB

Figure 5: Comparison of the results at the frequency of 770 Hz, without noise (a), and with SNR of -10 dB (b).

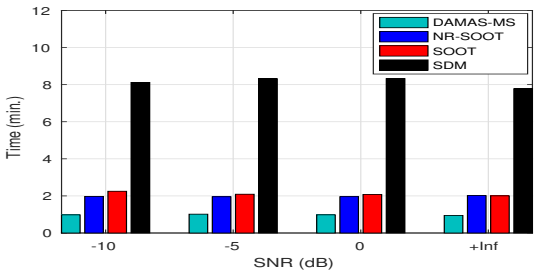

Figure 6: Computational times for input data without noise and for three different signal-to-noise ratios, SNR $\in \{-10, -5, 0\}$ dB.

appears, as indicated by the red arrows in Figure 7b. For the case of a SNR of -10 dB (Fig. 8), DAMAS-MS, SDM do not identify the sources and give many false alarms. The original SOOT manages to estimate a point source at the true source positions but also gives many false alarms. In contrast, the NR-SOOT algorithm still gives good results and provides the best performance compared to the three other methods.

Figure 6 shows the computational time (in minutes) for the different methods and for different noise levels. The computational time corresponds to the time required to satisfy the stopping criterion, i.e. $\|\mathbf{Q}^l - \mathbf{Q}^{l-1}\| \leq \sqrt{NF} \times 10^{-6}$, with the simulations performed on the same CPU. The SDM computational cost is four-fold the SOOT and NR-SOOT computational costs. As SDM is an approach that is similar to the forward-backward method, these results confirm the performance of the proposed majorant. In all cases, DAMAS-MS is the fastest algorithm, but the computational costs for DAMAS-MS, SOOT and NR-SOOT are of the same order (from 1-2 min).

To conclude, the NR-SOOT algorithms have better performances than the DAMAS-MS, SDM methods in terms of localization, as the source S_2 is spread over several x positions by DAMAS-MS and SDM, whereas the SOOT and the proposed NR-SOOT algorithm manage to estimate a point source at the true source position. Nevertheless, in term of robustness against noise, the NR-SOOT method is the only one that provides satisfactory results for low SNRs.

5.2. Real data

We finally compare the proposed NR-SOOT algorithm with the classical methods using real data. The experiment was conducted in January 2015 by DGA naval systems at Lake Castillon, a mountain lake in the French Alps with an average depth of 100 m and a maximum width of 600 m. This consisted of towing a 21-m-long scale model of a surface ship. The ship hull included two shakers, S_1 and S_2, that generated two point acoustic sources outside the hull: a sum of 3 sine functions at frequencies of 1200 Hz, 1400 Hz, and 1800 Hz, located at $x = -5.9m$, and a random broadband source located at $x = 2.3m$. A linear antenna of nine hydrophones that were equally spaced by 0.5 m recorded the propagated acoustic signals over $D = 14.15\,s$ for the source speed of $v = 2\,m/s$ (Fig. 9). We also consider the same configuration with the source speed of $v = 5\,m/s$ over $D = 5.3\,s$. (Fig. 10). The coordinate system of the array was used to describe all of

the geometries, with the origin corresponding to the array center. The array was immersed at $10\,m$ in depth and was positioned at $2.50\,m$ from the closest point of approach in the y direction. The source trajectory was calculated using a tachymeter system on the idler pulley. The acquisition time considered for the array processing is sufficient, such that the ship model passed by entirely above the antenna. In these Figures, the zones indicated in the red ellipses correspond to the estimated autospectrum of the sine source at the three frequencies of $1200\,Hz$, $1400\,Hz$, and $1800\,Hz$, and the red arrows show the remaining noise or the false alarms.

First, we consider the results in the case of the source speed $v = 2\,m/s$ (Fig. 9). The three methods improve the BF-MS output and identify the sources. DAMAS-MS and NR-SOOT have better performances than SDM in terms of localization. However, for the result of the DAMAS-MS method, there are some false alarms that are indicated by the red arrows in Figure 9b.

Secondly, we consider the case with the source speed $v = 5\,m/s$, for which the signal in the recording is more noisy. In this configuration, one new 'natural' source appears at the wake of the ship (Fig. 9d, bottom left). Three methods identify three sources, whereby the sine source is better localized by the NR-SOOT algorithm than the other methods. Both the DAMAS-MS and SDM methods show many false alarms, which are indicated by the red arrows in Figure 10b, c. In particular, the localization of the 'natural' source is only possible with the NR-SOOT algorithm. In conclusion, our results from this experiment remain true to our hypothesis, as well as our predictions. The results shown in Figure 9 and Figure 10 present the best results with perfect source location and improved robustness against noise for the NR-SOOT algorithm.

6. Conclusions

This paper proposes a new method, known as NR-SOOT, that is an extension of the SOOT algorithm [18], for moving-source localization based on blind deconvolution in underwater acoustic data. As the number of sources is small enough and they do not spread spatially, its autospectrum has a sparse representation, and it is possible to obtain more accurate results for blind deconvolution through a regularization function. The smooth approximation of ℓ_1/ℓ_2 shows very good performances in terms of localization and suppression of false alarms, and provides better results than DAMAS-MS and SDM, particularly for low SNRs.

Appendix

In this appendix, we give the explicit expressions of the proximity operators involved in the NR-SOOT algorithm. *For every* $(\mathbf{H}, \mathbf{Q}, \sigma^2) \in \mathbb{R}^{NF} \times \mathbb{R}^{NF} \times \mathbb{R}_+$ *and* $\gamma \in \,]0, +\infty[$, *let* G_1, G_2, *and* G_3 *be the majorant matrix of* ψ *at* $\mathbf{H}$, *at* $\mathbf{Q}$, *and at* σ^2, *respectively, that are given by Proposition 2. Then*

1. $\operatorname{prox}_{(\gamma_1)^{-1}G_1,\iota_C} = \Pi_C$,
2. $\operatorname{prox}_{(\gamma_2)^{-1}G_2,\iota_{[q_{\min},q_{\max}]^{NF}}} = \Pi_{[q_{\min},q_{\max}]^{NF}}$,
3. $\operatorname{prox}_{(\gamma_3)^{-1}G_3,\iota_{[\sigma^2_{\min},\sigma^2_{\max}]}} = \Pi_{[\sigma^2_{\min},\sigma^2_{\max}]}$,

which can be easily computed.

Acknowledgements

This work was financially supported by the Ministère du Redressement Productif (Direction Générale de la Compétitivité, de l'Industrie et des Services) and by the DGA-MRIS, grant RAPID ARMADA N°122906030.

References

[1] S. Haykin, Ed., *Blind Deconvolution*, Prentice Hall, 1994.

[2] A. K. Nandi, D. Mampel, and B. Roscher, "Blind deconvolution of ultrasonic signals in nondestructive testing applications," *IEEE Trans. Signal Process.*, vol. 45, no. 5, pp. 1382–1390, 1997.

[3] D. Kundur and D. Hatzinakos, "Blind image deconvolution," *IEEE Signal Process. Mag.*, vol. 13, no. 3, pp. 43–64, May 1996.

[4] M. Kato, I. Yamada, and K. Sakaniwa, "A set-theoretic blind image deconvolution based on hybrid steepest descent method," *IEICE Trans. Fund. Electron. Comm. Comput. Sci.*, vol. E82-A, no. 8, pp. 1443–1449, Aug. 1999.

[5] A. Ahmed, B. Recht, and J. Romberg, "Blind deconvolution using convex programming," *IEEE Trans. Inf. Theory*, vol. 60, no. 3, pp. 1711–1732, Mar. 2014.

[6] P. Campisi and K. Egiazarian, Eds., *Blind Image Deconvolution: Theory and Applications*, CRC Press, 2007.

[7] M. Zibulevsky and B. A. Pearlmutter, "Blind source separation by sparse decomposition in a signal dictionary," *Neural Comput.*, vol. 13, no. 4, pp. 863–882, Apr. 2001.

[8] N. Martins, S. Jesus, C. Gervaise, and A. Quinquis, "A time frequency approach to blind deconvolution in multipath underwater channels", *IEEE International Conference on Acoustics, Speech and Signal Processing (ICASSP 2002)*, Orlando, FL, 2002.

[9] K.-G. Sabra, H.-C. Song, and D.-R. Dowling, "Ray-based blind deconvolution in ocean sound channels", *The Journal of the Acoustical Society of America*, 127(2), EL42-EL47, 2004.

[10] S.-H. Abadi, H.-C. Song, and D.-R. Dowling, "Broadband sparse-array blind deconvolution using frequency-difference beamforming", *The Journal of the Acoustical Society of America*, 132(5), 3018-3029, 2012.

[11] A. Pereira, "Acoustic imaging in enclosed spaces", *Phd thesis*, Laboratoire de Vibro-acoustique , INSA Lyon, 2013.

[12] T. Suzuki, "L_1 generalized inverse beam-forming algorithm resolving coherent/incoherent, distributed and multipole sources", *Journal of Sound and Vibration*, vol. 330, no. 24, pp. 5835–5851, November 21, 2011.

[13] N. Chu, J. Picheral, A. Mohammad-Djafari, and N. Gac, "A robust super-resolution approach with sparsity constraint in acoustic imaging", *Applied Acoustics*, vol. 76, pp. 197–208, Feb. 2014.

[14] A. Benichoux, E. Vincent, and R. Gribonval, " A fundamental pitfall in blind deconvolution with sparse and shift-invariant priors," in *Proc. Int. Conf. on Acoustics, Speech, and Signal Process.*, Vancouver, Canada, May, 26-31, 2013.

[15] P. Comon, "Contrasts for multichannel blind deconvolution," *Signal Process. Lett.*, vol. 3, no. 7, pp. 209–211, Jul. 1996.

[16] É. Moreau and J.-C. Pesquet, "Generalized contrasts for multichannel blind deconvolution of linear systems," *Signal Process. Lett.*, vol. 4, no. 6, pp. 182–183, Jun. 1997.

[17] E. Esser, R. Wang, T. T.Y. Lin and F. J. Herrmann "Resolving scaling ambiguities with the ℓ_1/ℓ_2 norm in a blind deconvolution problem with feedback," in *IEEE workshop on Computational Advances in Multi-Sensor Adaptive Processing*, Cancun, Mexico, Dec., 2015.

[18] A. Repetti, M.-Q. Pham, L. Duval, E. Chouzenoux, and J.-C. Pesquet, "Euclid in a Taxicab: Sparse Blind Deconvolution with Smoothed ℓ_1/ℓ_2 Regularization", *IEEE Signal Processing Letters*, vol. 62, no. 16, pp. 539–543, August 15, 2014.

[19] R. J. Urick, " Principles of Underwater Sound", 3rd edition, Mc Graw-Hill Book Company, 1983.

[20] V. Fleury, J. Bulté, "Extension of deconvolution algorithms for the mapping of moving acoustic sources", *JASA.*, vol. 129, no. 3, pp. 1417–1428, March 2011.

[21] E. Vertatschitsch and S. Haykin, "Nonredundant arrays", *Proc. IEEE*, vol. 74, no. 1, pp. 217–218, January, 1986.

[22] A. T. Moffet, " Minimum-redundancy linear arrays", *IEEE Trans. Antennas Propagat.*, vol. 16, no. 2, pp. 172–175, Mar., 1968.

[23] R. P. Smith, "Constant beamwidth receiving arrays for broad band sonar systems", *Acta Acustica united with Acustica*, vol. 23, no. 1, pp. 21–26, January, 1970.

[24] B.D. Van Veen and K.M. Buckley, "Beamforming: a versatile approach to spatial filtering", *IEEE assp magazine*, vol. 5, no. 2, pp. 4–24, April, 1988.

[25] J. A. Högbom, "Aperture Synthesis with a Non-Regular Distribution of Interferometer Baselines", *Astron. Astrophys. Suppl.*, no. 15, pp. 417–426, 1974.

[26] J. Tsao and B. D. Steinberg, "Reduction of sidelobe and speckle artifacts in microwave imaging: the CLEAN technique", *IEEE Trans. Signal Process*, vol. 36, no. 4, pp. 543–556, Apr., 1988.

[27] P. Sijtsma, "CLEAN based on spatial source coherence", *International Journal of Aeroacoustics*, vol. 6, no. 4, pp. 357–374, 2007.

[28] S. G. Mallat and Z. Zhang, " Matching Pursuits with Time-Frequency Dictionaries", *IEEE Trans. Signal Process*, vol. 41, no. 12, pp. 3397–3415, December 1993.

[29] T. F. Brooks, and W. M. Humphreys, "Deconvolution approach for the mapping of acoustic sources (DAMAS) determined from phased microphone arrays", *Sound and Vibration*, vol. 294, pp. 856–879, 2006.

[30] T. Yardibi, J. Li, P. Stoica, L. Cattafesta, "Sparsity constrained deconvolution approaches for acoustic source mapping", *JASA*, vol. 123, no. 5, pp. 2631–2642, June 2008.

[31] S. Brühl, and A. Röder, "Acoustic noise source modelling based on microphone array measurements", *Journal of Sound and Vibration*, vol. 231, no. 3, pp. 611–617, March, 2000.

[32] A. L. Swindlehurst and T. Kailath, "A performance analysis of subspace-based methods in the presence of model errors. I. The MUSIC algorithm," *IEEE Trans. Signal Process.*, vol. 40, no. 7, pp. 1758–1774, Jul. 1992.

[33] V. Fleury, J. Bulté, and R. Davy, "Determination of acoustic directivity from microphone array measurements using correlated monopoles", *29th AIAA*, 5–7 May 2008, Vancouver, British Columbia Canada.

[34] K. Sun, Y. Liu, H. Meng, and X. Wang, "Adaptive Sparse Representation for Source Localization with Gain/Phase Errors", *Sensors*, vol. 11, no. 5, pp. 4780–4793, May 02, 2011.

[35] S. Cotter, B. Rao, K. Engan, and K. Kreutz, " Sparse solutions to linear inverse problems with multiple measurement vectors", *IEEE Trans. Signal Process*, vol. 53, no. 7, pp. 2477–2488, Jully 2005.

[36] D. M. Malioutov, M. Cetin, and A. S. Willsky, "A sparse signal reconstruction perspective for source localization with sensor arrays", *IEEE Trans. Signal Process*, vol. 53, no. 8, pp. 3010–3022, Aug., 2005.

[37] Y. Doisy, L. Deruaz and R. Been, "Interference suppression of subarray adaptive beamforming in presence of sensor dispersions," *IEEE Trans. Signal Process.*, vol. 58, no. 8, pp. 4195–4212, Apr. 2010.

[38] J. Chen and X. Huo, "Sparse Representations for Multiple Measurement Vectors (MMV) in an Over-Complete Dictionary", *ICASSP 2005*, Philadelphia, PA, USA., pp. 257–260, March 2005.

[39] B. Oudompheng, B. Nicolas and L. Lamotte, "Passive synthetic aperture array to improve noise mapping of a moving ship", *OCEANS 2015*, Genova, Italy, pp. 1–6, May 18-21, 2015.

[40] B. Oudompheng, "Localisation et contribution de sources acoustiques de navire au passage par traitement d'antenne réduite", *Phd thesis*, GIPSA-Lab, 2015.

[41] M.-Q. Pham, B. Oudompheng, B. Nicolas and J.- I. Mars, "Sparse deconvolution for moving-source localization", *IEEE International Conference on Acoustics, Speech and Signal Processing (ICASSP 2016)*, Shanghai, China, March 20-25, 2016, pp. 355–359.

[42] S. H. Abadi, D. Rouseff, D. R Dowling, "Blind deconvolution for robust signal estimation and approximate source localization", *Journal of the Acoustical Society of America*, vol. 131, no. 4, pp. 2599–2610, Apr., 2012.

[43] J. Bolte, P. L. Combettes, and J.-C. Pesquet, "Alternating proximal algorithm for blind image recovery," in *Proc. Int. Conf. Image Process.*, Hong-Kong, China, Sep. 26-29, 2010, pp. 1673–1676.

[44] E. Chouzenoux, J.-C. Pesquet, and A. Repetti, "A block coordinate variable metric forward-backward algorithm," *J. Global Optimization, Springer Verlag*, pp.1-29, 2016.

[45] J. Bolte, S. Sabach, and M. Teboulle, "Proximal alternating linearized minimization fon nonconvex and

nonsmooth problems," *Math. Progr. (Ser. A)*, Jul. 2013.
[46] E. Chouzenoux, J.-C. Pesquet, and A. Repetti, "Variable metric forward-backward algorithm for minimizing the sum of a differentiable function and a convex function", *J. Optim. Theory Appl.*, vol. 162, no. 1, pp. 107–132, Jul. 2014.
[47] M. W. Jacobson and J. A. Fessler, "An expanded theoretical treatment of iteration-dependent Majorize-Minimize algorithms," *IEEE Trans. Image Process.*, vol. 16, no. 10, pp. 2411–2422, Oct. 2007.
[48] P. L. Combettes and B. C. Vũ, "Variable metric quasi-Fejér monotonicity," *Nonlinear Anal.*, vol. 78, pp. 17–31, Feb. 2013.
[49] H. H Bauschke and P. L. Combettes, "Convex analysis and monotone operator theory in hilbert spaces," *Springer Verlag New York*, 2011.
[50] P. L. Combettes and J.-C. Pesquet, "Proximal splitting methods in signal processing", *in Fixed-point algorithms for inverse problems in science and engineering*, H. H. Bauschke, R. Burachik, P. L. Combettes, V. Elser, D. R. Luke, and H. Wolkowicz, Eds., pp. 185–212. Springer Verlag, 2011.

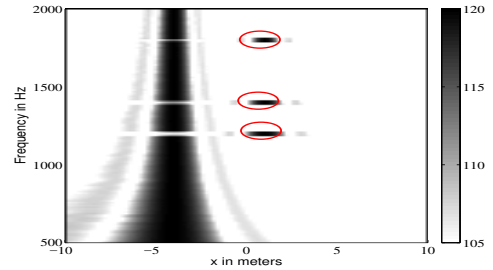

(a) Initial BF-MS

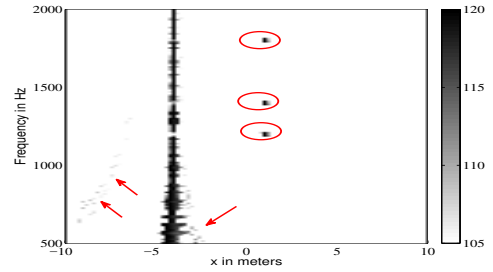

(b) Deconvolution with DAMAS-MS

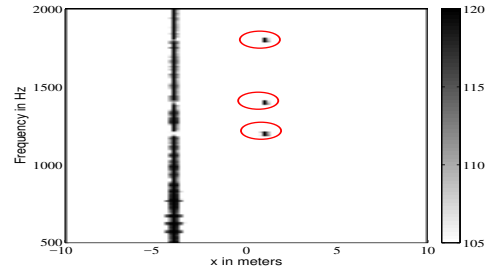

(c) Deconvolution with SDM

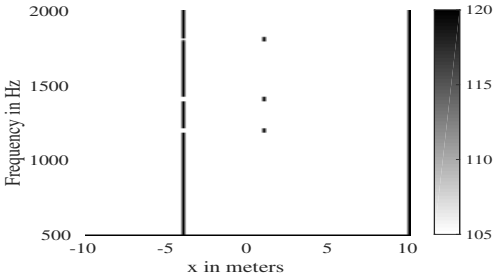

(d) Blind deconvolution with SOOT

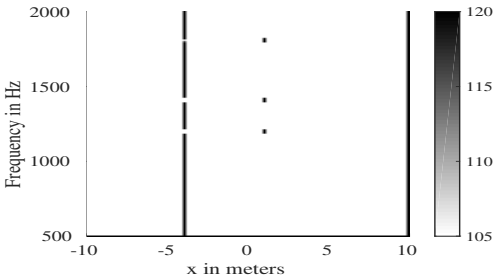

(e) Blind deconvolution with NR-SOOT

Figure 7: Localization in the frequency-distance domain obtained (in the case without noise). (a) Initial BF-MS. (b) DAMAS-MS. (c) SDM. (d) original SOOT. (e) NR-SOOT (the dynamic ranges shown are 15 dB).

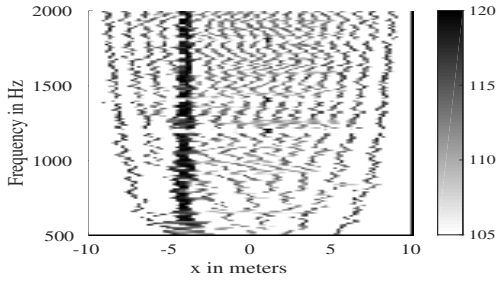

(a) Initial BF-MS

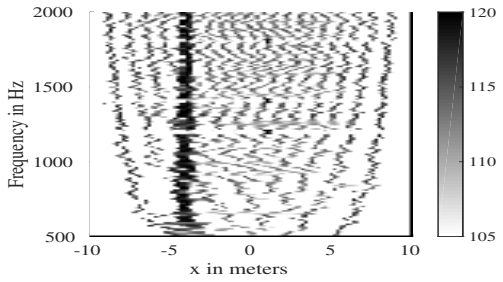

(b) Deconvolution with DAMAS-MS

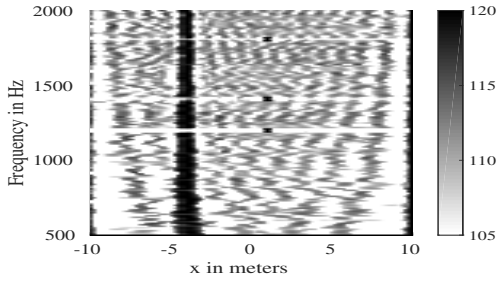

(c) Deconvolution with SDM

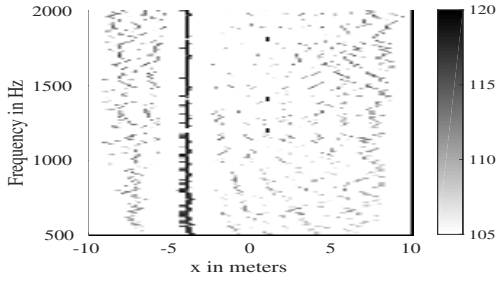

(d) Blind deconvolution with SOOT

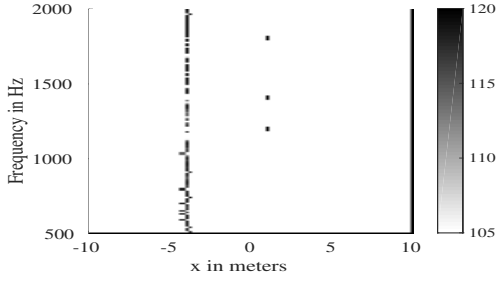

(e) Blind deconvolution with NR-SOOT

Figure 8: Localization in the frequency-distance domain obtained (with SNR of -10 dB). (a) Initial BF-MS. (b) DAMAS-MS. (c) SDM. (d) original SOOT. (e) NR-SOOT (the dynamic ranges shown are 15 dB).

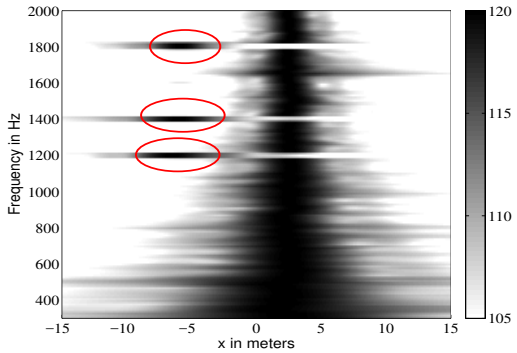

(a) Initial BF-MS

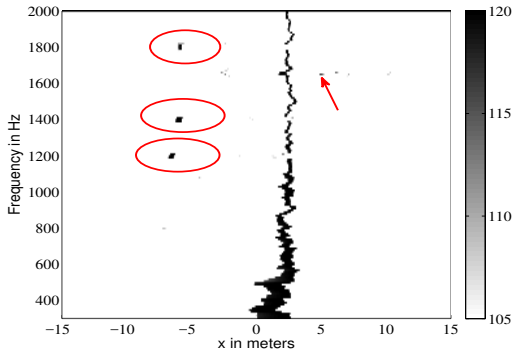

(b) Deconvolution with DAMAS-MS

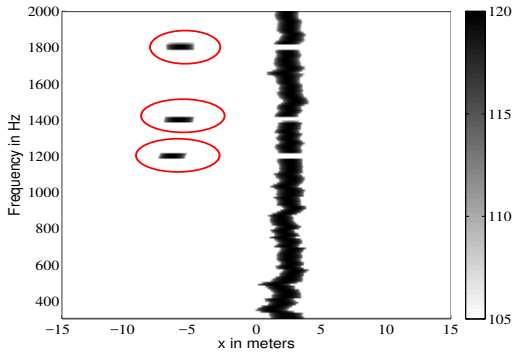

(c) Deconvolution with SDM

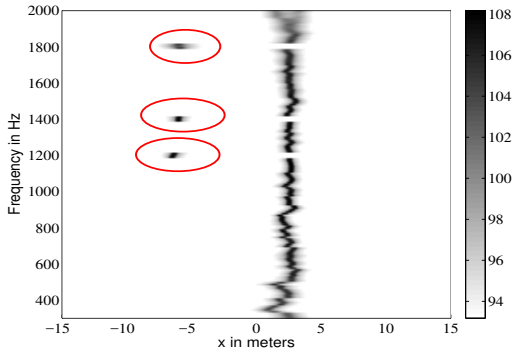

(d) Blind deconvolution with NR-SOOT

Figure 9: Localization obtained in the frequency-distance domain for the model ship with two artificial sources, traveling at 2 m/s. (a) Initial BF-MS. (b) DAMAS-MS. (c) SDM. (d) NR-SOOT (the dynamic ranges shown are 15 dB).

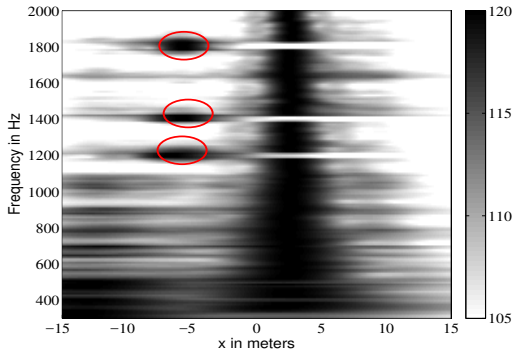

(a) Initial BF-MS

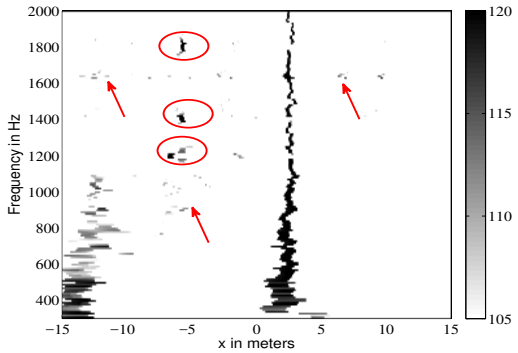

(b) Deconvolution with DAMAS-MS

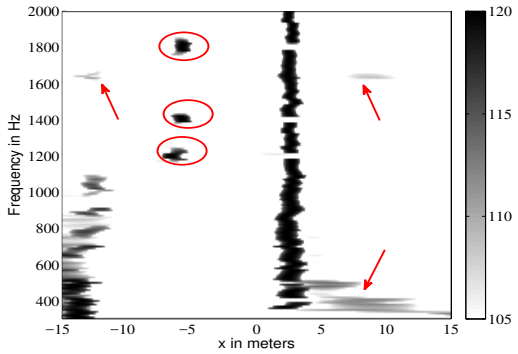

(c) Deconvolution with SDM

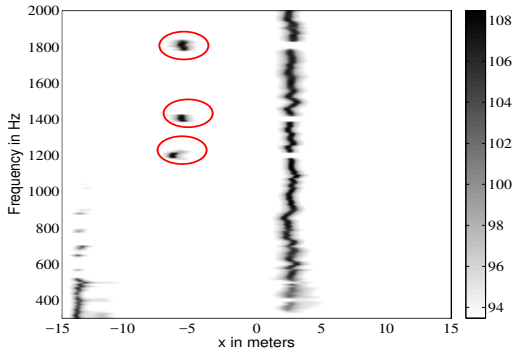

(d) Blind deconvolution with NR-SOOT

Figure 10: Localization obtained in the frequency-distance domain for the model ship with two artificial sources, traveling at 5 m/s. (a) Initial BF-MS. (b) DAMAS-MS. (c) SDM. (d) NR-SOOT (the dynamic ranges shown are 15 dB).